Rapid Assembly of Amyloid-β Peptide at a Liquid/Liquid Interface Produces Unstable β-Sheet Fibers†

Michael R. Nichols,*,‡,§ Melissa A. Moss,‡,|| Dana Kim Reed,‡ Jan H. Hoh,⊥ and Terrone L. Rosenberry‡

Department of Neuroscience, Mayo Clinic College of Medicine, 4500 San Pablo Road, Jacksonville, Florida 32224, and Department of Physiology, Johns Hopkins University School of Medicine, 725 North Wolfe Street, Baltimore, Maryland 21205

Received June 4, 2004; Revised Manuscript Received August 30, 2004

ABSTRACT: Accumulation of aggregated amyloid-β peptide (Aβ) in the brain is a pathological hallmark of Alzheimer's disease (AD). In vitro studies indicate that the 40- to 42-residue Aβ peptide in solution will undergo self-assembly leading to the transient appearance of soluble protofibrils and ultimately to insoluble fibrils. The Aβ peptide is amphiphilic and accumulates preferentially at a hydrophilic/hydrophobic interface. Solid surfaces and air−water interfaces have been shown previously to promote Aβ aggregation, but detailed characterization of these aggregates has not been presented. In this study Aβ(1−40) introduced to aqueous buffer in a two-phase system with chloroform aggregated 1−2 orders of magnitude more rapidly than Aβ in the buffer alone. The interface-induced aggregates were released into the aqueous phase and persisted for 24−72 h before settling as a visible precipitate at the interface. Thioflavin T fluorescence and circular dichroism analyses confirmed that the Aβ aggregates had a β-sheet secondary structure. However, these aggregates were far less stable than Aβ(1−40) protofibrils prepared in buffer alone and disaggregated completely within 3 min on dilution. Atomic force microscopy revealed that the aggregates consisted of small globules 4−5 nm in height and long flexible fibers composed of these globules aligned roughly along a longitudinal axis, a morphology distinct from that of Aβ protofibrils prepared in buffer alone. The relative instability of the fibers was supported by fiber interruptions apparently introduced by brief washing of the AFM grids. To our knowledge, unstable aggregates of Aβ with β-sheet structure and fibrous morphology have not been reported previously. Our results provide the clearest evidence yet that the intrinsic β-sheet structure of an in vitro Aβ aggregate depends on the aggregation conditions and is reflected in the stability of the aggregate and the morphology observed by atomic force microscopy. Resolution of these structural differences at the molecular level may provide important clues to the further understanding of amyloid formation in vivo.

Alzheimer's disease (AD)[1] is a complex disorder manifested by progressive dementia and inexorable death. Pathological hallmarks of AD include deposition of insoluble fibrillar amyloid aggregates in the brain parenchyma and cerebral vessels (see ref *1*). The primary component of these amyloid deposits is the amyloid-β peptide (Aβ). Aβ is also found as soluble 40- and 42-residue peptides in cerebrospinal fluid (*2*) and plasma (*3*). These peptides, denoted Aβ(1−40) and Aβ(1−42), are generated by proteolytic processing of the amyloid precursor protein (APP). Several hypotheses have been offered to account for AD. The amyloid hypothesis, which has considerable support from a wide array of genetic, animal, and biochemical studies, maintains that accumulation of aggregated Aβ is the primary cause of the disease (*4*).

The most striking evidence supporting the amyloid hypothesis comes from the identification of numerous mutations linked to early-onset familial AD (FAD) (*5*). These mutations are located within the APP gene or the genes for presenilins 1 and 2, which play an integral role in APP processing and Aβ production. All FAD mutations reported thus far increase either the overall production of Aβ, the level of the more amyloidogenic Aβ(1−42) relative to Aβ(1−40) (reviewed in ref *5*), or the propensity of a mutated Aβ to form amyloid aggregates (*6*). Taken as a whole, these findings underscore the importance of understanding the biophysical properties of Aβ peptides and identifying conditions that affect Aβ aggregation.

Aβ aggregation is difficult to study in vivo, but it has been explored extensively in vitro, where it involves noncovalent self-assembly of monomers to form fibrils characteristic of those found in post-mortem AD brains (*7*). This assembly process is inferred to be nucleation-dependent (*8*), because solutions of Aβ monomers display a detectable lag phase prior to the onset of aggregation. The nuclei serve as seeds

† This work was supported by awards from the American Heart Association, Florida/Puerto Rico Affiliate (to M.R.N. and M.A.M.).

* To whom correspondence should be addressed. Telephone: 314-516-7345. Fax: 314-516-5342. E-mail: nicholsmic@umsl.edu.

‡ Mayo Clinic College of Medicine.

§ Current address: Department of Chemistry and Biochemistry, University of Missouri−St. Louis, St. Louis, MO 63121-4400.

|| Current address: Department of Chemical Engineering, University of South Carolina, Columbia, SC 29208.

⊥ Johns Hopkins University School of Medicine.

[1] Abbreviations: AD, Alzheimer's disease; AFM, atomic force microscopy; APP, amyloid precursor protein; DLS, dynamic light scattering; FAD, early-onset familial AD; HFIP, hexafluoro-2-propanol; PC, phosphatidylcholine; PG, phosphatidylglycerol; PS, phosphatidylserine; SEC, size exclusion chromatography; SM, sphingomyelin.

10.1021/bi048846t CCC: $30.25
Published on Web 12/10/2004

for immediate and rapid monomer deposition in a polydisperse mixture of soluble protofibrils (*9*). The protofibrils grow and coalesce to complete the formation of mature insoluble fibrils (*10*). The lag time prior to nucleation can be eliminated by introduction of tiny amounts of sonicated Aβ fibrils to serve as templates for linear polymerization (*11*). Protofibrillar and fibrillar Aβ structures possess high β-sheet content (*12*) with the β-strands arranged perpendicular to the long axis of the fibril (*13*). Molecular models of Aβ fibril structure invoke both hydrogen-bonding and hydrophobic interactions between peptide side chains based on data from solid-state NMR (*14*), hydrogen exchange (*15*, *16*), and polymerization (*17*) studies.

The process of Aβ nucleation remains an open and important question. Aβ aggregation rates can be variable in solution and are sensitive to many conditions including pH, ionic strength, temperature, and agitation (*9*, *18*). Several reports have indicated that, in addition to hydrophobic interactions, amphipathic properties may also drive nucleation. Some studies have identified micellar-like Aβ structures and suggested that they may play a role in nucleation (*19*−*21*). The potential for Aβ micelles arises from the Aβ sequence itself, which contains a hydrophobic C-terminal region and a largely hydrophilic N-terminal region. The amphiphilic molecular structure imparts surfactant-like properties to Aβ as determined by the ability to lower the surface tension of water (*22*). Surface-active molecules tend to accumulate at interfaces between water and nonpolar liquids (*23*), resulting in a concentration increase at the interface compared to the bulk solvent phase.

Based on the amphiphilic structure of Aβ and experimental data indicating Aβ surface activity, it was of interest to determine how Aβ interaction at a defined liquid/liquid interface influences the rate of aggregation and the structure of the aggregates. In this report, we show that the Aβ(1−40) aggregation rate was dramatically enhanced at an aqueous solution/chloroform interface and that the aggregate structure and stability were notably distinct from those of Aβ(1−40) protofibrils prepared in buffer alone.

EXPERIMENTAL PROCEDURES

Materials. Aβ(1−40) peptide was purchased from QCB (Hopkinton, MA). [^{3}H]HCHO was from American Radiolabeled Chemicals Inc. (10 Ci/mmol), scintillation cocktail (Ultima Gold) was from Packard, thioflavin T was from Sigma, and chloroform (Optima >99.9%) was from Fisher Scientific. The peptide KLVFF-K_6 was synthesized by the protein and peptide core facility at Mayo Clinic (Rochester, MN) using standard Fmoc techniques (*24*).

Aβ Preparations. The Aβ peptide was obtained in lyophilized form and stored desiccated at −20 °C until reconstitution in 50 mM Tris-HCl (pH 8.0). Any preexisting aggregates were removed by size exclusion chromatography (SEC) on Superdex 75 equilibrated in 5 or 50 mM Tris-HCl (pH 8.0). In most cases, 5 mM EDTA−NaOH (pH 8.0) was added to this buffer (denoted 5 or 50 mM Tris−EDTA) to minimize any degradation of Aβ to smaller peptides (*18*). Aβ was radiolabeled for use in some experiments by reductive methylation with [^{3}H]HCHO and $NaCNBH_3$ (*18*). Unlabeled HCHO was added to attain a 10 mM total concentration, which ensured complete conversion of the α-amino group of D1 and the ϵ-amino groups of K16 and K28 to ^{3}H-labeled dimethylamines (*18*). Radioactivity was determined by scintillation counting, and the specific activity of the SEC-purified [^{3}H]Aβ(1−40) preparations used in this study were 380−460 dpm/pmol. Concentrations of low molecular weight Aβ obtained from SEC were determined with an extinction coefficient of 1450 cm^{-1} M^{-1} at 276 nm (*18*). The monomeric nature of this Aβ was confirmed by multiangle light scattering in tandem with SEC. This analysis was conducted with radiomethylated Aβ for better quantitation and indicated a M_w of 4670 ± 90 (calculated M_w of 4415 for the hexamethylated 1−40 peptide) (*25*). The monomeric assignment was in agreement with translational diffusion measurements by NMR (*26*).

Two-Phase Aβ Aggregation. An interfacial system was constructed by adding 0.2 mL of chloroform to a 9 × 30 mm glass vial (Fisher Scientific). Aqueous buffer (0.2−0.3 mL) was then added to the chloroform, and if necessary, the vial was briefly centrifuged at 2000*g* to better define separation between the two phases. Aβ was introduced to the upper aqueous phase, and the system was incubated at room temperature without agitation. Aβ aggregation was monitored by thioflavin T fluorescence as described previously (*18*). This fluorophore shows greatly enhanced fluorescence on binding to amyloid fibrils formed by a number of peptides and proteins (*27*), although it also forms fluorescent complexes with some nonamyloid proteins (e.g., ref *28*). During the time course of the aggregation, successive 10 μL aliquots from the center of the aqueous phase were diluted into a Tris buffer (pH 8.0) containing 5 μM thioflavin T. Fluorescence emission (F) at 480 nm was monitored at 23 °C on a Perkin-Elmer LS-50B luminescence spectrometer with excitation at 450 nm.

Dynamic Light Scattering (DLS). Hydrodynamic radius (R_H) measurements were made at room temperature with a DynaPro MSX instrument (Protein Solutions, Piscataway, NJ) (*18*). Samples (60 μL) were placed directly into a quartz cuvette, and light scattering intensity at a 90° angle was collected using a 20 s acquisition time. Particle diffusion coefficients were calculated from autocorrelated light intensity data and converted to R_H with the Stokes−Einstein equation. Mean R_H values were determined over 20 s data acquisition intervals and included contributions from the solvent. Data regularization with Dynamics software (version 5.26.60) separated distinct particle populations and generated histograms of percent intensity vs R_H. Intensity-weighted mean R_H values were derived from these regularized histograms.

Circular Dichroism. Samples (0.3 mL) were placed into a rectangular quartz cuvette with a 0.1 cm path length (Hellma). Spectra were obtained by wavelength scan from 260 to 190 nm using an Aviv Model 215 circular dichroism spectrometer, and three successive wavelength scans were averaged for each Aβ sample. Buffer control spectra were averaged and subtracted from Aβ sample spectra, and each resulting point ($[\theta]_{obs}$, deg) was converted to mean residue ellipticity ($[\theta]$, deg cm^2 $dmol^{-1}$) with the equation $[\theta] = [\theta]_{obs}(MRW/10lc)$, where MRW is the mean residue molecular weight of Aβ(1−40) (4331 g/mol divided by 40 residues), l is the optical path length (cm), and c is the concentration (g/cm^3). Secondary structure estimates were obtained using the modified Contin method (CONTINLL)

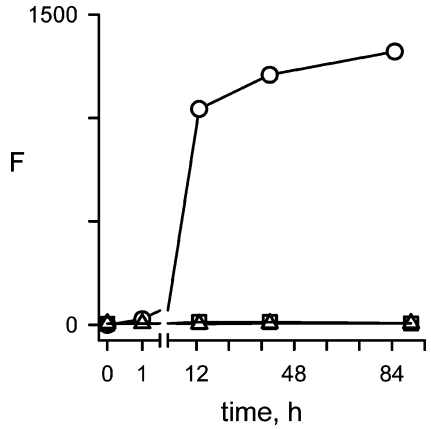

FIGURE 1: Accelerated rate of aggregation for Aβ at an aqueous solution/chloroform interface. A two-phase system was established as described in the Experimental Procedures with chloroform and an aqueous phase containing 55 μM monomeric Aβ(1−40) in 5 mM Tris−EDTA. Aβ aggregation was monitored at periodic time points with a thioflavin T fluorescence assay (F, ○) (see Experimental Procedures). Two single-phase incubations without chloroform were also assessed. These consisted of Aβ(1−40) in 5 mM Tris−EDTA (□) and Aβ(1−40) in 5 mM Tris−EDTA that was presaturated with chloroform by shaking and gentle centrifugation (△). Data points represent single measurements, but the results are representative of six two-phase experiments and two experiments for each single-phase incubation.

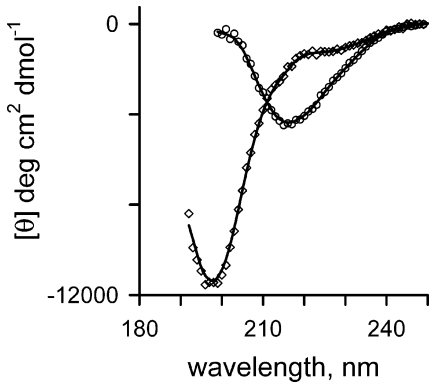

FIGURE 2: Circular dichroism spectra of Aβ aggregates generated in the two-phase system. A sample removed from an aqueous phase containing 50 μM Aβ(1−40) in 5 mM Tris-HCl (pH 8.0) that had been incubated over a chloroform phase for 24 h was analyzed by circular dichroism as described in the Experimental Procedures. Raw data (symbols) were fit with a smoothed line generated in SigmaPlot software. Spectra for stock monomeric Aβ (◇) and the aqueous phase aggregates (○) are compared.

available through the CDPro suite of analysis programs. Basis set 7 of the reference protein database (*29*) was used to estimate percentages of Aβ secondary structure from unsmoothed data collected from 260 to 199 nm for aggregate and from 260 to 190 nm for monomer.

Atomic Force Microscopy (AFM). Images were obtained as described previously (*18*). In brief, samples were incubated for 15 min on freshly cleaved mica that had been modified with 3′-(aminopropyl)triethoxysilane (APTES), and the disk was washed briefly with water. A Nanoscope III controller with a Multimode AFM (Digital Instruments, Santa Barbara, CA) was used for imaging. Height images were "flattened", and particle height distributions were obtained with NanoScope (R) III software (version 5.13r5; Digital Instruments). Heights vs line distance were displayed on a horizontal or vertical line section through the image.

RESULTS

The Formation of Aβ(1−40) Aggregates with a β-Sheet Structure Is Significantly Accelerated at an Aqueous Solution/Chloroform Interface. A liquid/liquid two-phase system was established in order to test the hypothesis that the amphiphilicity of Aβ may influence fibril formation. The introduction of monomeric Aβ(1−40) (hereafter referred to as Aβ) to the upper aqueous phase of an aqueous solution/chloroform two-phase system dramatically accelerated the rate of aggregation as measured by thioflavin T fluorescence compared to the same concentration of Aβ in aqueous buffer alone (Figure 1). The time required for the characteristic lag phase was reduced from several weeks to hours. Although the solubility of chloroform in water is low (<1%), the possibility that even a slight miscibility between chloroform and the aqueous layer may have contributed to the aggregation rate enhancement was addressed by adding Aβ to an aqueous solution that was previously saturated with chloroform. Aβ aggregation in this preparation showed an extremely long lag time similar to that of Aβ in untreated aqueous buffer (Figure 1). Clearly, the presence of the defined liquid/liquid interface was critical for the accelerated aggregation. The aggregates were apparently not fixed at the interface but released into the bulk aqueous phase, because aliquots for aggregation measurements were taken a substantial molecular distance (~2−3 mm) from the interface.

An enhancement of thioflavin T fluorescence typically suggests binding to an amyloid structure rich in β-sheet, and the circular dichroism spectrum of the bulk aqueous phase aggregates after 24 h confirmed this point (Figure 2). A single minimum was present at 216 nm, and deconvolution with a standard program (*29*) indicated a preponderance of β-structure (sheet and turn). The circular dichroism spectrum of the monomeric Aβ solution before addition to this two-phase system corresponded largely to unstructured random coil.

Interfacial Aggregation Is Highly Concentration-Dependent. We hypothesized that accumulation of the Aβ peptide at the aqueous solution/chloroform interface contributed to the dramatic enhancement of its nucleation and subsequent aggregation. If the extent of accumulation depended on the concentration of Aβ in the aqueous phase, the rate of aggregation should be concentration-dependent. To probe this question, the Aβ concentration was varied and the effect on lag phase kinetics was analyzed (Figure 3). Increasing the Aβ monomer concentration markedly reduced the lag phase prior to aggregation. Lag times declined from 5 to 0.4 h as the Aβ concentration was increased from 20 to 80 μM. The acute sensitivity of the lag phase to concentration supported our idea that Aβ accumulation at a liquid/liquid interface can play an important role in Aβ nucleation kinetics.

Interface-Induced Aggregates Are Very Unstable. A surprising finding was the relative instability of the Aβ aggregates formed in the presence of the aqueous solution/chloroform interface. We have described previously the formation of soluble protofibrils in a conventional aggregation reaction in low ionic strength buffer at pH 8.0 (*18*). These protofibrils disaggregated only slightly after a 3 day incubation and 30-fold dilution (*25*), and this slow disaggregation is in agreement with a previous report (*12*). Aβ

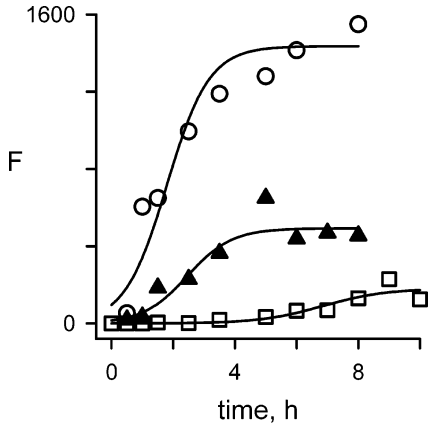

FIGURE 3: Dependence of interfacial aggregation on Aβ concentration. Separate two-phase samples were established with chloroform and an aqueous phase of 30 mM Tris-HCl (pH 8.0) containing increasing Aβ(1−40) concentrations (20 μM, □; 40 μM, ▲; and 80 μM, ○), and aliquots from the aqueous phase were monitored for thioflavin T fluorescence (F) over time. Aggregation kinetic parameters were obtained by fitting data points to the sigmoidal curve $F = a/[1 + \exp(-(t - t_0)/b)]$ (*40*) using Sigma Plot 8.0. In this equation t is time, a and b are fixed parameters, and t_0 is the time to reach half-maximal thioflavin T fluorescence. Data points were weighted by $1/y^{0.5}$, and lines correspond to the fitted curves. Lag times were determined using the method described in ref *40* and were equal to $t_0 - 2b$ for each fitted curve. Results are representative of three experiments.

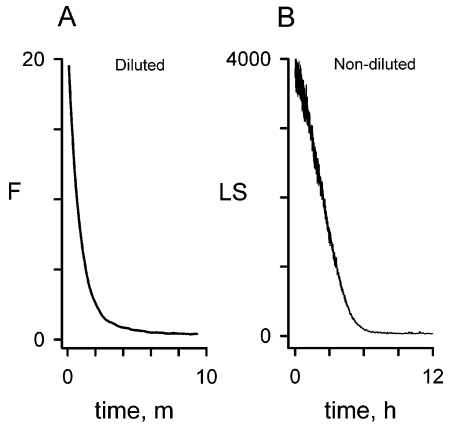

FIGURE 4: Stability of Aβ aggregates generated in the two-phase system. A two-phase system established with chloroform and an aqueous phase containing 30 μM Aβ(1−40) in 50 mM Tris-HCl (pH 8.0) was incubated for 30 h. An aliquot was removed from the aqueous phase and diluted 15-fold into the same buffer containing 5 μM thioflavin T for measurement of fluorescence (F) (panel A) or analyzed without dilution in a sealed cuvette by DLS (panel B). DLS measurement of 90° light scattering intensity (LS), which is presented in kilocounts and dependent on laser power, was monitored continuously.

aggregates removed from the aqueous phase after a 1 day incubation in this two-phase system disaggregated rapidly following 15-fold dilution into buffer containing thioflavin T. Fluorescence levels corresponding to the diluted aggregates rapidly declined to background in less than 10 min (Figure 4A). Furthermore, simply removing an aliquot of the aqueous phase from the interface was sufficient to induce essentially complete disaggregation. Total light scattering intensity, which is dependent on both particle concentration and size, diminished significantly during this time from over 4000 to 30 kilocounts (Figure 4B). These DLS measurements indicated that initial aggregates dispersed in the aqueous phase were quite large, with an intensity-weighted R_H value of 250 nm, but this R_H value decreased only slightly over the time course in Figure 4B because of a very small population of more stable aggregates. However, aqueous phase aliquots from some preparations gave R_H histograms that gradually resolved into two peaks with the smaller, predominant mass peak corresponding to the R_H for monomer. SEC analysis of a radiomethylated Aβ sample at this point confirmed that the radiolabeled Aβ eluted from Superdex 75 primarily as monomer (86%) with the remainder corresponding to smaller degradation products (data not shown). The finding that levels of the aggregates could persist for up to 96 h in the aqueous phase suspended over the chloroform phase yet were relatively unstable when an aliquot of this aqueous phase was removed from the system suggested a dynamic equilibrium in which aggregation initiated at the interface was balanced by disaggregation in the bulk aqueous phase.

We used AFM to compare the structures of Aβ aggregates formed in the two-phase system with those of Aβ protofibrils that had been elongated by deposition of monomer following aggregation in our conventional low ionic strength buffer (*18*). We define protofibrils as soluble aggregates (i.e., aggregates that do not sediment after 10 min centrifugation at 18000*g*) and often further restrict protofibril size by isolating those recovered in the void volume following SEC. The mixture of globular aggregates and short rods (3−4 nm in height and <1 μm length) revealed by AFM analysis of our Aβ protofibrils (*18*) appears very similar to AFM images of early Aβ protofibrils (*30*) and Aβ(1−42) oligomers (*31*) obtained by others, despite differences in aggregate preparation. For the comparison here, we first elongated isolated Aβ protofibrils by brief deposition of Aβ monomers. As described previously, the resulting soluble elongated protofibrils included long wispy tendrils extending to lengths of several micrometers (*18*). We then removed residual monomer by SEC and recovered the subset of shorter elongated protofibrils shown in Figure 5A,D. They consisted of rodlike filaments with an average height of 3.1 nm, often emanating from globular cores that were typical of the protofibrils prior to elongation (*18*). AFM images of the two-phase aggregates (Figure 5B,E and 5C,F) revealed structures that we denote flexible fibers, with lengths of much greater than 1 μm, as well as numerous species that appeared globular. The fibers appeared to be composed of a collection of the globular species aligned roughly along a longitudinal axis. This is highlighted by the inset in Figure 5B,E, which clearly shows several globules associating to form a small fiber. The measured heights for both fibers and globules in Figure 5E were similar, with a mean height of 4.6 ± 1.5 nm (SD) for the fibers and 4.0 ± 1.8 nm for the globules. Distinctions between the elongated protofibrils in Figure 5A,D and the two-phase aggregate sample in Figure 5B,E and 5C,F are clear: the two-phase aggregates included no rodlike filaments, and the elongated protofibrils showed no chainlike alignment of globules. Furthermore, Figure 5F showed discontinuities within central sections of several fibers. These discontinuities, visible in both the amplitude and height modes, were not artifacts arising from tracking of the AFM tip on the horizontal fast scan axis. Such artifacts can occur but result in apparent fiber breaks only in the amplitude mode. Rather, the discontinuities appeared to reflect disag-

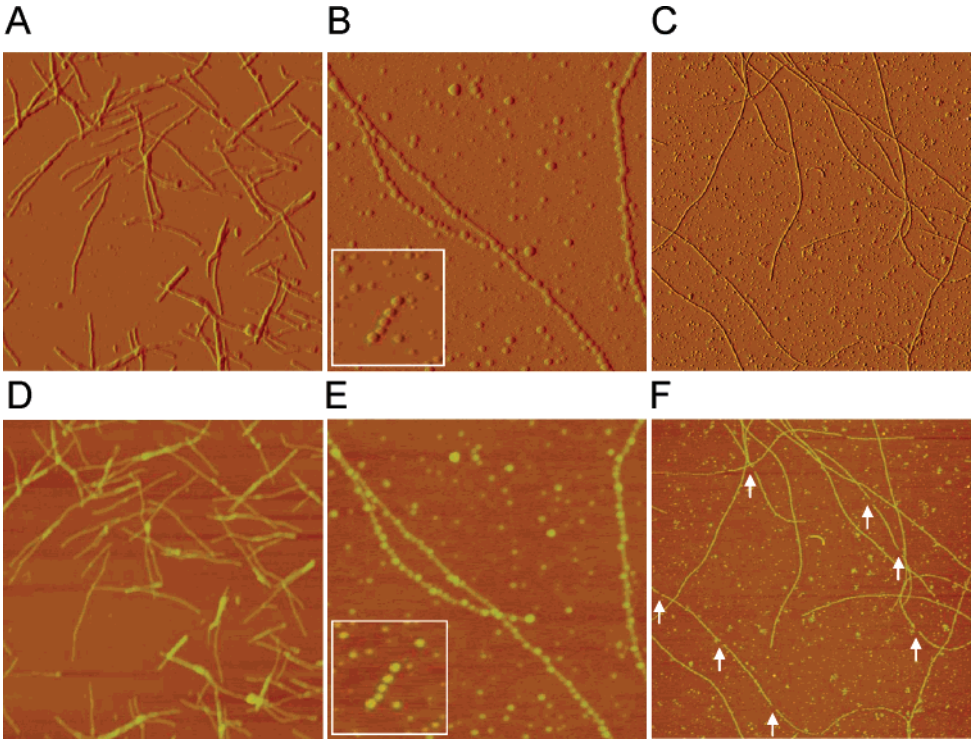

FIGURE 5: Comparison of structures of Aβ aggregates induced in the two-phase system with those of Aβ protofibrils by AFM. Images are presented in both amplitude mode (panels A−C) and height mode (panels D−F), where increasing brightness indicates greater damping of cantilever oscillation or increasing feature height, respectively (*9*). Panels A and D: Aβ(1−40) protofibrils were prepared by vigorous continued vortexing of monomeric Aβ (180 μM) in 5 mM Tris−EDTA overnight at room temperature (*18*). The protofibrils were elongated by incubation with monomeric Aβ (30 μM) for 0.5 h and isolated a second time by SEC (*18*). A 100 μL sample (1 μM in Aβ monomer units) was applied to the mica surface. Panels B, C, E, and F: Aβ aggregates were induced in a two-phase system with chloroform and an aqueous phase containing 50 μM Aβ(1−40) in 50 mM Tris-HCl (pH 8.0) that was incubated for 24 h. A 20 μL aliquot from the aqueous phase was diluted 5-fold with 50 mM Tris-HCl (pH 8.0) directly on the mica surface. Images are 2.5 μm^2 (panels A, B, D, and E; insets in B and E are on this same scale) or 10 μm^2 (panels C and F). Images and insets in panels B, C, E, and F were taken from locations in close proximity to each other on the same sample grid. Arrows in panel F indicate areas of fiber discontinuity.

gregation of individual globular components of the fibers during adsorption of the diluted sample and washing of the AFM disk. Such rapid disaggregation is consistent with the fiber instability in the aqueous phase shown in Figure 4.

The Latter Stages of Aggregation Involve Precipitation of Fibrils on the Interface. Aggregation induced by the liquid/liquid interface in Figure 1 varied among different preparations but typically reached maximum levels between 24 and 96 h. In every case, this peak was followed by a rapid decline in aggregate concentration in the aqueous phase as measured by the thioflavin T fluorescence of sample aliquots. Continued incubation produced a cloudy white precipitate hovering at and just above the aqueous solution/chloroform interface. The experiments were repeated with radiomethylated Aβ to provide a more quantitative measure of aqueous concentrations during the aggregation time course. This modification slows the assembly kinetics but does not affect the morphology of protofibrils or fibrils (*18*). A biphasic decline of radioactivity from the aqueous phase coincided with both the initial increase and the later decrease in Aβ aggregates measured by fluorescence (Figure 6). The rapid initial loss of radioactivity from the aqueous phase suggested accumulation of monomer at the interface during the lag phase prior to aggregate formation. The radioactivity plateau from approximately 24−48 h was consistent with dual processes of continued monomer accumulation at the interface and new aggregate diffusion back into the bulk aqueous phase. The precipitation of larger insoluble aggregates from the aqueous phase onto the interface later in the aggregation reaction was indicated by further loss of radioactivity and complete loss of thioflavin T fluorescence in the aqueous phase. A single-phase aqueous solution of radiolabeled Aβ in a control vial showed no measurable loss of radioactivity after 170 h. This confirmed that loss of labeled Aβ in the two-phase system was not due to nonspecific adsorption of the peptide to the walls of the vial (data not shown).

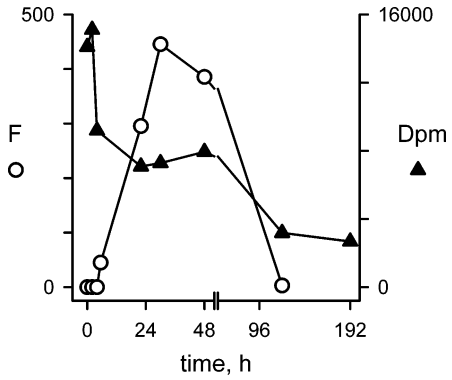

FIGURE 6: Precipitation of Aβ fibrils at the two-phase interface. A two-phase system was established with chloroform and an aqueous phase containing 25 μM [^{3}H]Aβ(1−40) in 50 mM Tris−EDTA. Aliquots of the aqueous phase were taken for measurements of thioflavin T fluorescence (F, ○) and radioactivity (dpm, ▲) at the indicated incubation times. Results are representative of five experiments.

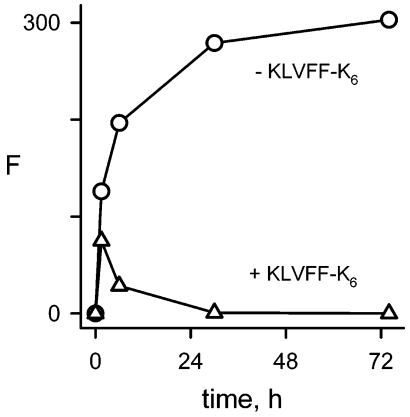

FIGURE 7: Promotion of large Aβ aggregate formation by the peptide KLVFF-K_6. Two-phase systems were established with chloroform and an aqueous phase of 50 mM Tris−EDTA with or without KLVFF-K_6 (30 μM final concentration). [^{3}H]Aβ(1−40) was added to the aqueous phase to a final concentration of 30 μM, and aliquots of the aqueous phase were taken for measurements of thioflavin T fluorescence (F) at the indicated incubation times in the presence (△) or absence (○) of KLVFF-K_6. Results are representative of two experiments.

The peptide KLVFF-K_6 includes residues 16−20 of the Aβ sequence modified with a C-terminal hexalysine tag. This small peptide does not aggregate but has been found to stimulate the formation of large Aβ aggregates (*32*) and, more specifically, to dramatically accelerate association of Aβ protofibrils to form mature insoluble fibrils (*24*). Incubation of both radiolabeled Aβ and KLVFF-K_6 at equimolar concentrations in the aqueous phase of a two-phase system resulted in only a transient appearance of soluble aggregates (Figure 7), yet significant interfacial Aβ precipitates were visible by 6 h. A rapid loss of radioactivity from the aqueous phase reached 90% by 72 h and confirmed a marked decrease in Aβ concentration (data not shown). Clearly, the presence of KLVFF-K_6 in the aqueous phase accelerated Aβ precipitation relative to that of the control reaction without KLVFF-K_6 in Figure 7. The elimination of a relatively extended thioflavin T fluorescence maximum and a biphasic radioactivity decline was in sharp contrast to the transient accumulation of smaller soluble aggregates typically observed when KLVFF-K_6 was not included.

DISCUSSION

The amphipathic character of Aβ predicts that the peptide will preferentially accumulate at the interface between two liquids with disparate dielectric constants. The question of how this type of interfacial environment influences Aβ aggregation kinetics has not been addressed and was the basis for this study. The data were striking and clearly showed that Aβ aggregation rates were vastly accelerated at an aqueous solution/chloroform interface compared to Aβ in bulk solution. Lag times prior to measurable aggregate formation were decreased from weeks to several hours. The interface-induced aggregates exhibited several features in common with Aβ fibrils and protofibrils formed in bulk solution, including significant β-sheet structure, polydisperse morphologies that involved long fibers and short globular species, and accelerated formation of insoluble aggregates in the presence of KLVFF-K_6. However, important differences also were observed among these preparations. AFM images indicated that the long fibers formed in the two-phase system retained the appearance of distinct globules aligned along a longitudinal axis, in contrast to the more uniform rodlike extensions of the elongated protofibrils. Furthermore, these fibers disaggregated much more rapidly than protofibrils when they were removed from contact with the interface. The interface-induced Aβ aggregation differs from that in homogeneous aqueous solutions (*18*) by its accelerated rate and extremely dynamic equilibrium between large aggregate formation and disaggregation. Therefore, the structure of these rapidly formed fiber aggregates must differ, perhaps in only subtle ways, from the Aβ protofibrils and fibrils that form slowly in solution with a high degree of structural order approaching that observed in protein crystals (*33*).

Other studies have focused on amyloid formation at aqueous solution/air (*34*) and aqueous solution/solid interfaces (*35*, *36*). Schladitz et al. established an air/water interface by spreading an alkaline Aβ solution in a monolayer over a pure water subphase. Infrared reflection/absorption spectroscopy revealed a rapid and substantial increase in the interfacial β-sheet content compared to that of a similar incubation in bulk solution (*34*). Zhu et al. investigated aggregation of an aqueous solution of the light chain variable domain (SMA) on a mica surface. The assembly of SMA aggregates occurred at much lower protein concentrations, and the rates of aggregation were markedly accelerated relative to those in bulk solution (*35*). A liquid/liquid interface may influence Aβ conformation and aggregation in a much different way than a liquid/solid interface. Nevertheless, our studies of Aβ aggregation at an aqueous solution/chloroform interface extend these previous reports by following the aggregation time course in its entirety through nucleation, polymerization, and precipitation and by analyzing soluble aggregates after diffusion from the interface into the aqueous phase.

Aβ aggregations typically display two features of nucleated growth polymerization, namely, a kinetic lag phase and a contraction or loss of the lag phase by seeding with preformed fibrils. Nucleated growth polymerization also can involve a striking dependence on the monomer concentration. For example, the length of the lag phase for deoxyhemoglobin S polymerization is dependent on approximately the 30th power of the monomer concentration (*37*), and this has been interpreted as indicating a homogeneous nucleus size of approximately seven monomers (*38*). It is likely that interfacial accumulation of Aβ at an aqueous solution/chloroform interface increases the rate of peptide encounters and thereby contributes to nucleation and the accelerated aggregation rate we observed. The extent of Aβ accumulation at the interface is difficult to estimate. The cross-sectional area of phospholipid molecules in bilayers is nearly 1 nm^2 (*39*), and interfacial Aβ molecules even in extended conformations are unlikely to exceed this density. In our experimental system, this would correspond to a maximum of 10^{14} Aβ molecules at the interface, about 2 orders of magnitude smaller than the total Aβ introduced to the aqueous phase. The fact that our data in Figure 3 show a strong correlation between aggregation rates and aqueous phase Aβ concentration suggests that Aβ is a weak amphiphile that does not reach a saturating density at the interface (see discussion below). More importantly, the concentration dependence of this interfacial aggregation

appears to be more pronounced than the concentration dependence of nucleation for several amyloidogenic peptides in solution. The length of the lag phase for insulin fibril formation decreased by a factor of 6 over a 100-fold increase in insulin concentration (*40*), and no change in lag phase length was observed over a 10-fold range of amylin (IAPP) concentrations (*41*). Furthermore, the kinetics of the initial phase of nucleation of polyglutamine peptides indicated that the nucleus was monomeric (*42*). To our knowledge, no systematic investigation of the concentration dependence of the length of the lag phase for Aβ aggregation in solution has been reported. If in fact this dependence were lower than that at the interface, one might infer a difference in the mechanisms of nucleation in the one- and two-phase systems.

In addition to an increased Aβ concentration at the aqueous solution/chloroform interface, the role of Aβ ordering and/or folding in promoting aggregation cannot be overlooked. Pratt and Pohorille (*23*) point out in their review of aqueous solution interfaces that while the main feature of solute interfacial behavior is the tendency to accumulate at the interface, increased rigidity and ordering can also occur for flexible amphiphilic solutes at the interface compared to that in aqueous solution. Furthermore, it was noted that many unstructured peptides and small proteins in aqueous solution adopt ordered structures at an interface. The interface may induce a particular orientation or conformation favorable for aggregation. The possibility that a folding event drives amyloid formation has been raised recently by Wetzel and colleagues from studies of polyGln aggregation. These studies suggested that the rate-limiting nucleation step might be energetically unfavorable monomer folding that creates an energetically favorable pathway to oligomer formation (*42*). It is likely that both increased Aβ concentration and an altered Aβ conformation at the interface play a role in the significant enhancement of Aβ aggregation rate in an interfacial system.

In our model of Aβ aggregation at the aqueous solution/chloroform interface, monomer accumulation at the interface promotes nucleus formation. Polymerization then occurs by addition of monomer from the aqueous phase and/or from a monomer pool already associated at the interface. During this interfacial growth, many aggregates are released from the interface and diffuse into the aqueous phase. Most of the released aggregates that are stable enough to be detected correspond to the isolated globular species observed by AFM. Growth also can be promoted by direct association of the aggregates in the buffer phase, and this process is likely to contribute to the fiber structures in the AFM images. The peptide KLVFF-K_6 has been shown to dramatically accelerate the association of Aβ protofibrils in solution (*24*), and the fact that KLVFF-K_6 also strongly promoted the insolubility of these interfacial aggregates indicated that this post-nucleation Aβ growth mechanism applies both to these aggregates and to Aβ protofibrils. Eventually, through interfacial growth and aggregate association, insoluble aggregates precipitate and sediment at the interface. The rapid growth and instability of these interfacial aggregates are of particular interest in the context of our recent demonstration of dramatically accelerated Aβ aggregation in dilute hexafluoro-2-propanol (HFIP) (1−4%) (*25*). The HFIP-induced Aβ aggregates, like the interfacial aggregates described here, contained primarily β-sheet structure according to their circular dichroism spectra, formed globular species that progressed to fibers as observed by AFM, and rapidly disaggregated on dilution. These striking similarities may be explained at least in part by our recent observation that HFIP in dilute aqueous solution forms microdroplets that can be observed by EM and partially sedimented by centrifugation (*25*). The formation of a second phase by these microdroplets is consistent with a report of hydrated HFIP oligomers in dilute HFIP solutions (*43*).

It is unclear whether the enhanced interfacial formation of unstable Aβ aggregates revealed in our studies has physiological relevance. The cellular environment offers a variety of interfaces that could promote Aβ aggregation, and interface-promoted aggregation could help to reconcile amyloid formation at the low Aβ concentrations found in vivo (0.25−3 nM) (*3*) with the micromolar concentrations of Aβ necessary for in vitro aggregation in solution (*30*, *44*). At least one other class of amphiphilic biomolecule is believed to exploit interfacial aggregation. Hydrophobins are small fungal proteins important for fungal growth and development and are the most surface-active proteins known (*45*). Excreted as water-soluble monomers, hydrophobins can be found as highly insoluble aggregates in the walls of the aerial hyphae (*46*). These 10 nm diameter aggregates, called rodlets, have been recapitulated in vitro at air/water and oil/water interfaces (*46*, *47*). Molecular dynamics simulations at a water/hexane interface indicate that the hydrophobin SC3 undergoes rapid folding to form extensive β-sheet structure (*45*). The most obvious cellular interfaces are provided by phospholipid membranes, and some studies have examined mixtures of organic and aqueous solvents as models of biological membranes. Miscible water/alcohol mixtures have been used to model the effects of membrane fields on α-synuclein aggregation (*48*), and the aqueous solution/chloroform interface, which promotes accumulation of amphiphiles in an interfacial monolayer, has been used to investigate protein interactions with phospholipid monolayers (*49*). More direct studies of the effects of phospholipid vesicles on Aβ aggregation also have been conducted. Neutral phospholipid vesicles composed of phosphatidylcholine (PC) or sphingomyelin (SM) did not promote a β-sheet conformation of Aβ in solution (*50*), and addition of cholesterol to PC or PC/PS vesicles did not induce Aβ binding (*51*, *52*). In contrast, anionic phospholipid vesicles enriched in phosphatidylglycerol (PG) (*53*) as well as G_{M1} ganglioside micelles and PC/G_{M1} vesicles (*50*, *54*) promoted Aβ binding and β-sheet content. However, Aβ interactions with these vesicles appeared restricted to the lipid polar headgroups without insertion of amphiphilic Aβ into the hydrophobic core of the bilayer (*53*, *55*, *56*). Insertion of Aβ into PC/PG monolayers was observed at a lateral pressure (20 mN/m) lower than that in bilayers (32 mN/m), indicating that Aβ is a weak amphiphile with only modest surface activity (*53*). The water/chloroform interface presents a more hydrophobic surface for Aβ interaction than phospholipid mono- or bilayers, and possible physiological sources of hydrophobic surfaces are worth noting. For example, lipoprotein particles may provide a more accessible physiological source of a hydrophobic interface than phospholipid membranes. While submicromolar concentrations of apolipoprotein E inhibit Aβ fibril formation in vitro, higher concen-

trations promote complexes of this apolipoprotein with thioflavin T-positive Aβ aggregates (*57*).

The findings in this study expand our understanding of the biophysical properties of Aβ and factors that can affect Aβ assembly. The accumulation and resulting aggregation of Aβ at the aqueous solution/chloroform interface raise the question of whether hydrophobic surfaces or hydrophilic/hydrophobic interfaces can facilitate in vivo Aβ protofibril and fibril formation. Furthermore, identification of amyloid species with similar macroscopic structural features but marked differences in stability indicates a level of molecular complexity that has not previously been appreciated.

ACKNOWLEDGMENT

We acknowledge members of Professor Art Edison's laboratory at the University of Florida, Gainesville, for the use of their circular dichroism instrument and their assistance in data acquisition. We also acknowledge Stephanie Cratic-McDaniel in the laboratory of Professor Jan H. Hoh at Johns Hopkins University for assistance in atomic force microscope imaging of our samples.

REFERENCES

1. Selkoe, D. J. (1994) Normal and abnormal biology of the β-amyloid precursor protein, *Annu. Rev. Neurosci. 17*, 489−517.
2. Shoji, M., Golde, T. E., Ghiso, J., Cheung, T. T., Estus, S., Shaffer, L. M., Cai, X. D., McKay, D. M., Tintner, R., Frangione, B., and Younkin, S. G. (1992) Production of the Alzheimer amyloid β protein by normal proteolytic processing, *Science 258*, 126−129.
3. Seubert, P., Vigo-Pelfrey, C., Esch, F., Lee, M., Dovey, H., Davis, D., Sinha, S., Schlossmacher, M., Whaley, J., Swindlehurst, C., McCormack, R., Wolfert, R., Selkoe, D. J., Lieberberg, I., and Schenk, D. (1992) Isolation and quantification of soluble Alzheimer's β-peptide from biological fluids, *Nature 359*, 325−327.
4. Hardy, J., and Selkoe, D. J. (2002) The amyloid hypothesis of Alzheimer's disease: Progress and problems on the road to therapeutics, *Science 297*, 353−356.
5. Selkoe, D. J., and Podlisny, M. B. (2002) Deciphering the genetic basis of Alzheimer's disease, *Annu. Rev. Genomics Hum. Genet. 3*, 67−99.
6. Nilsberth, C., Westlind-Danielsson, A., Eckman, C. B., Condron, M. M., Axelman, K., Forsell, C., Stenh, C., Luthman, J., Teplow, D. B., Younkin, S. G., Naslund, J., and Lannfelt, L. (2001) The "Artic" APP mutation (E693G) causes Alzheimer's disease by enhanced Aβ protofibril formation, *Nat. Neurosci. 4*, 887−893.
7. Kirschner, D. A., Inouye, H., Duffy, L. K., Sinclair, A., Lind, M., and Selkoe, D. J. (1987) Synthetic peptide homologous to β protein from Alzheimer disease forms amyloid-like fibrils *in vitro*, *Proc. Natl. Acad. Sci. U.S.A. 84*, 6953−6957.
8. Jarrett, J. T., and Lansbury, P. T., Jr. (1993) Seeding "one-dimensional crystallization" of amyloid: a pathogenic mechanism in Alzheimer's disease and scrapie?, *Cell 73*, 1055−1058.
9. Harper, J. D., Wong, S. S., Lieber, C. M., and Lansbury, P. T., Jr. (1999) Assembly of Aβ amyloid peptides: An *in vitro* model for a possible early event in Alzheimer's disease, *Biochemistry 38*, 8972−8980.
10. Harper, J. D., Lieber, C. M., and Lansbury, P. T., Jr. (1997) Atomic force microscopic imaging of seeded fibril formation and fibril branching by the Alzheimer's disease amyloid-β protein, *Chem. Biol. 4*, 951−959.
11. Jarrett, J. T., Berger, E. P., and Lansbury, P. T., Jr. (1993) The carboxy terminus of the beta amyloid protein is critical for the seeding of amyloid formation: implications for the pathogenesis of Alzheimer's disease, *Biochemistry 32*, 4693−4697.
12. Walsh, D. M., Hartley, D. M., Kusumoto, Y., Fezoui, Y., Condron, M. M., Lomakin, A., Benedek, G. B., Selkoe, D. J., and Teplow, D. B. (1999) Amyloid β-protein fibrillogenesis: Structure and biological activity of protofibrillar intermediates, *J. Biol. Chem. 274*, 25945−25952.
13. Sikorski, P., Atkins, E. D., and Serpell, L. C. (2003) Structure and texture of fibrous crystals formed by Alzheimer's Aβ(11−25) peptide fragment, *Structure (Cambridge) 11*, 915−926.
14. Petkova, A. T., Ishii, Y., Balbach, J. J., Antzutkin, O. N., Leapman, R. D., Delaglio, F., and Tycko, R. (2002) A structural model for Alzheimer's β-amyloid fibrils based on experimental constraints from solid-state NMR, *Proc. Natl. Acad. Sci. U.S.A. 99*, 16742−16747.
15. Kraus, M., Bienert, M., and Krause, E. (2003) Hydrogen exchange studies on Alzheimer's amyloid-β peptides by mass spectrometry using matrix-assisted laser desorption/ionization and electrospray ionization, *Rapid Commun. Mass. Spectrom. 17*, 222−228.
16. Kheterpal, I., Zhou, S., Cook, K. D., and Wetzel, R. (2000) Aβ amyloid fibrils possess a core structure highly resistant to hydrogen exchange, *Proc. Natl. Acad. Sci. U.S.A. 97*, 13597−13601.
17. Tjernberg, L. O., Naslund, J., Lindqvist, F., Johansson, J., Karlstrom, A. R., Thyberg, J., Terenius, L., and Nordstedt, C. (1996) Arrest of β-amyloid fibril formation by a pentapeptide ligand, *J. Biol. Chem. 271*, 8545−8548.
18. Nichols, M. R., Moss, M. A., Reed, D. K., Lin, W.-L., Mukhopadhyay, R., Hoh, J. H., and Rosenberry, T. L. (2002) Growth of β-amyloid(1−40) protofibrils by monomer elongation and lateral association. Characterization of distinct products by light scattering and atomic force microscopy, *Biochemistry 41*, 6115−6127.
19. Lomakin, A., Chung, D. S., Benedek, G. B., Kirschner, D. A., and Teplow, D. B. (1996) On the nucleation and growth of amyloid β-protein fibrils: Detection of nuclei and quantification of rate constants, *Proc. Natl. Acad. Sci. U.S.A. 93*, 1125−1129.
20. Tjernberg, L. O., Pramanik, A., Bjorling, S., Thyberg, P., Thyberg, J., Nordstedt, C., Berndt, K. D., Terenius, L., and Rigler, R. (1999) Amyloid β-peptide polymerization studied using fluorescence correlation spectroscopy, *Chem. Biol. 6*, 53−62.
21. Yong, W., Lomakin, A., Kirkitadze, M. D., Teplow, D. B., Chen, S. H., and Benedek, G. B. (2001) Structure determination of micelle-like intermediates in amyloid β-protein fibril assembly by using small angle neutron scattering, *Proc. Natl. Acad. Sci. U.S.A. 99*, 150−154.
22. Soreghan, B., Kosmoski, J., and Glabe, C. (1994) Surfactant properties of Alzheimer's A beta peptides and the mechanism of amyloid aggregation, *J. Biol. Chem. 269*, 28551−28554.
23. Pratt, L. R., and Pohorille, A. (2002) Hydrophobic effects and modeling of biophysical aqueous solution interfaces, *Chem. Rev. 102*, 2671−2692.
24. Moss, M. A., Nichols, M. R., Reed, D. K., Hoh, J. H., and Rosenberry, T. L. (2003) The peptide KLVFF-K_6 promotes β-amyloid(1−40) protofibril growth by association but does not alter protofibril effects on cellular reduction of 3-(4,5-dimethylthiazol-2-yl)-2,5-diphenyltetrazolium bromide (MTT), *Mol. Pharmacol. 64*, 1160−1168.
25. Nichols, M. R., Moss, M. A., Reed, D. K., Hoh, J. H., and Rosenberry, T. L. (2004) Amyloid-β protofibrils differ from amyloid-β aggregates induced in dilute hexafluoroisopropanol in stability and morphology, *J. Biol. Chem.* Papers in Press, http://dx.doi.org/10.1074/jbc.M410553200.
26. Tseng, B. P., Esler, W. P., Clish, C. B., Stimson, E. R., Ghilardi, J. R., Vinters, H. V., Mantyh, P. W., Lee, J. P., and Maggio, J. E. (1999) Deposition of monomeric, not oligomeric, Aβ mediates growth of Alzheimer's disease amyloid plaques in human brain preparations, *Biochemistry 38*, 10424−10431.
27. LeVine, H., III (1999) Quantification of β-sheet amyloid fibril structures with thioflavin T, *Methods Enzymol. 309*, 274−284.
28. De Ferrari, G. V., Mallender, W. D., Inestrosa, N. C., and Rosenberry, T. L. (2001) Thioflavin T is a fluorescent probe of the acetylcholinesterase peripheral site that reveals conformational interactions between the peripheral and acylation sites, *J. Biol. Chem. 276*, 23282−23287.
29. Sreerama, N., and Woody, R. W. (2000) Estimation of protein secondary structure from circular dichroism spectra: comparison of CONTIN, SELCON, and CDSSTR methods with an expanded reference set, *Anal. Biochem. 287*, 252−260.
30. Harper, J. D., Wong, S. S., Lieber, C. M., and Lansbury, P. T., Jr. (1997) Observation of metastable Aβ amyloid protofibrils by atomic force microscopy, *Chem. Biol. 4*, 119−125.
31. Stine, W. B. J., Dahlgren, K. N., Krafft, G. A., and LaDu, M. J. (2003) *In vitro* characterization of conditions for amyloid-β peptide oligomerization and fibrillogenesis, *J. Biol. Chem. 278*, 11612−11622.
32. Pallitto, M. M., Ghanta, J., Heinzelman, P., Kiessling, L. L., and Murphy, R. M. (1999) Recognition sequence design for peptidyl

modulators of β-amyloid aggregation and toxicity, *Biochemisty 38*, 3570−3578.
33. Tycko, R. (2003) Insights into the amyloid folding problem from solid-state NMR, *Biochemistry 42*, 3151−3159.
34. Schladitz, C., Vieira, E. P., Hermel, H., and Mohwald, H. (1999) Amyloid-β-sheet formation at the air−water interface, *Biophys. J. 77*, 3305−3310.
35. Zhu, M., Souillac, P. O., Ionescu-Zanetti, C., Carter, S. A., and Fink, A. L. (2002) Surface-catalyzed amyloid fibril formation, *J. Biol. Chem. 277*, 50914−50922.
36. Kowalewski, T., and Holtzman, D. M. (1999) *In situ* atomic force microscopy study of Alzheimer's β-amyloid peptide on different substrates: New insights into mechanism of β-sheet formation, *Proc. Natl. Acad. Sci. U.S.A. 96*, 3688−3693.
37. Hofrichter, J., Ross, P. D., and Eaton, W. A. (1974) Kinetics and mechanism of deoxyhemoglobin S gelation: a new approach to understanding sickle cell disease, *Proc. Natl. Acad. Sci. U.S.A. 71*, 4864−4868.
38. Cao, Z., and Ferrone, F. A. (1996) A 50th order reaction predicted and observed for sickle hemoglobin nucleation, *J. Mol. Biol. 256*, 219−222.
39. Costigan, S. C., Booth, P. J., and Templer, R. H. (2000) Estimations of lipid bilayer geometry in fluid lamellar phases, *Biochim. Biophys. Acta 1468*, 41−54.
40. Nielsen, L., Khurana, R., Coats, A., Frokjaer, S., Brange, J., Vyas, S., Uversky, V. N., and Fink, A. L. (2001) Effect of environmental factors on the kinetics of insulin fibril formation: Elucidation of the molecular mechanism, *Biochemistry 40*, 8397−8409.
41. Padrick, S. B., and Miranker, A. D. (2002) Islet amyloid: Phase partitioning and secondary nucleation are central to the mechanism of fibrillogenesis, *Biochemistry 41*, 4694−4703.
42. Chen, S., Ferrone, F. A., and Wetzel, R. (2002) Huntington's disease age-of-onset linked to polyglutamine aggregation nucleation, *Proc. Natl. Acad. Sci. U.S.A. 99*, 11884−11889.
43. Yoshida, K., Yamaguchi, T., Adachi, T., Otomo, T., Matsuo, D., Takamuku, T., and Nishi, N. (2003) Structure and dynamics of hexafluoroisopropanol−water mixtures by X-ray diffraction, small-angle neutron scattering, NMR spectroscopy, and mass spectrometry, *J. Chem. Phys. 119*, 6132−6142.
44. Lomakin, A., Teplow, D. B., Kirschner, D. A., and Benedek, G. B. (1997) Kinetic theory of fibrillogenesis of amyloid β-protein, *Proc. Natl. Acad. Sci. U.S.A. 94*, 7942−7947.
45. Zangi, R., de Vocht, M. L., Robillard, G. T., and Mark, A. E. (2002) Molecular dynamics study of the folding of hydrophobin SC3 at a hydrophilic/hydrophobic interface, *Biophys. J. 83*, 112−124.
46. Wosten, H., De Vries, O., and Wessels, J. (1993) Interfacial self-assembly of a fungal hydrophobin into a hydrophobic rodlet layer, *Plant Cell 5*, 1567−1574.
47. Wosten, H. A., Schuren, F. H., and Wessels, J. G. (1994) Interfacial self-assembly of a hydrophobin into an amphipathic protein membrane mediates fungal attachment to hydrophobic surfaces, *EMBO J. 13*, 5848−5854.
48. Munishkina, L. A., Phelan, C., Uversky, V. N., and Fink, A. L. (2003) Conformational behavior and aggregation of α-synuclein in organic solvents: Modeling the effects of membranes, *Biochemistry 42*, 2720−2730.
49. Wu, J., Li, J. B., Zhao, J., and Miller, R. (2000) Dynamic characterization of phospholipid/protein competitive adsorption at the aqueous solution/chloroform interace, *Colloids Surf., A 175*, 113−120.
50. Choo-Smith, L. P., and Surewicz, W. K. (1997) The interaction between Alzheimer amyloid β(1−40) peptide and ganglioside GM1-containing membranes, *FEBS Lett. 402*, 95−98.
51. Kakio, A., Nishimoto, S., Yanagisawa, K., Kozutsumi, Y., and Matsuzaki, K. (2001) Cholesterol-dependent formation of GM1 ganglioside-bound amyloid β-protein, an endogenous seed for Alzheimer amyloid, *J. Biol. Chem. 276*, 24985−24990.
52. Curtain, C. C., Ali, F. E., Smith, D. G., Bush, A. I., Masters, C. L., and Barnham, K. J. (2003) Metal ions, pH, and cholesterol regulate the interactions of Alzheimer's disease amyloid-β peptide with membrane lipid, *J. Biol. Chem. 278*, 2977−2982.
53. Terzi, E., Holzemann, G., and Seelig, J. (1997) Interaction of Alzheimer β-amyloid peptide(1−40) with lipid membranes, *Biochemistry 36*, 14845−14852.
54. Choo-Smith, L. P., Garzon-Rodriguez, W., Glabe, C. G., and Surewicz, W. K. (1997) Acceleration of amyloid fibril formation by specific binding of Aβ-(1−40) peptide to ganglioside-containing membrane vesicles, *J. Biol. Chem. 272*, 22987−22990.
55. Matsuzaki, K., and Horikiri, C. (1999) Interactions of amyloid β-peptide(1−40) with ganglioside-containing membranes, *Biochemistry 38*, 4137−4142.
56. Yip, C. M., and McLaurin, J. (2001) Amyloid-β peptide assembly: A critical step in fibrillogenesis and membrane disruption, *Biophys. J. 80*, 1359−1371.
57. Chan, W., Fornwald, J., Brawner, M., and Wetzel, R. (1996) Native complex formation between apolipoprotein E isoforms and the Alzheimer's disease peptide A beta, *Biochemistry 35*, 7123−7130.

BI048846T